

Robust Deep Reinforcement Learning via Multi-View Information Bottleneck

Jiameng Fan¹ Wenchao Li¹

Abstract

Deep reinforcement learning (DRL) agents are often sensitive to visual changes that were unseen in their training environments. To address this problem, we introduce a robust representation learning approach for RL. We introduce an auxiliary objective based on the multi-view information bottleneck (MIB) principle which encourages learning representations that are both predictive of the future and less sensitive to task-irrelevant distractions. This enables us to train high-performance policies that are robust to visual distractions and can generalize to unseen environments. We demonstrate that our approach can achieve SOTA performance on challenging visual control tasks, even when the background is replaced with natural videos. In addition, we show that our approach outperforms well-established baselines on generalization to unseen environments using the large-scale Procgen benchmark.

1. Introduction

In reinforcement learning (RL), learning control from raw images in an end-to-end fashion is important for many applications. While deep reinforcement learning can train agents to control effectively from image inputs, it suffers from problems of overfitting to training environments (Zhang et al., 2018b;a; Yu et al., 2019). In particular, it has been observed that DRL agents perform poorly in environments different from those where the agents were trained on, even when they are semantically equivalent to the training environment (Farebrother et al., 2018; Cobbe et al., 2019). By contrast, humans are able to adapt to new, unseen environments with similar underlying dynamics. For example, though visual observations can be drastically different when driving in different cities, human drivers quickly adjust to driving in a new city which they have never visited. We argue that humans can adapt to new scenarios because their

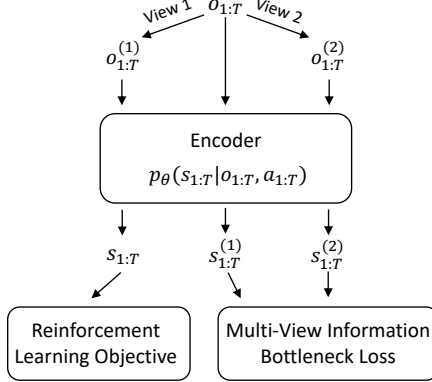


Figure 1: Robust Deep Reinforcement Learning via Multi-View Information Bottleneck (DRIBO) incorporates the inherent sequential structure of reinforcement learning and multi-view information bottleneck principle into robust representation learning in RL. We consider sequential multi-view observations, $\mathbf{o}_{1:T}^{(1)}$ and $\mathbf{o}_{1:T}^{(2)}$, of original sequential observation $\mathbf{o}_{1:T}$ sharing the same *task-relevant* information while any information not shared by them are *task-irrelevant*. DRIBO uses a multi-view information bottleneck loss to ensure that $s_{1:T}^{(1)}$ and $s_{1:T}^{(2)}$, the representations of multi-view observations, share maximal task-relevant information while eliminating the task-irrelevant information. DRIBO trains the RL policy and (or) value function on top of the encoder.

driving skills are invariant to predominantly visual details that are not relevant to driving. Conversely, DRL agents without this ability are hindered from understanding the underlying *task-relevant* dynamics and thus can be distracted by *task-irrelevant* visual details (Zhang et al., 2021).

Viewing from a representation learning perspective, a desired representation for RL should encode only task-relevant information in the environment, such as lane markings on the road for driving, while discarding excessive, task-irrelevant information, such as shape of the cloud in the sky. An RL agent that learns from such representations has the advantage of being more *robust to visual changes*. In addition, the resulting policy is more likely to *generalize to unseen environments* if the task-relevant information in the new environment remains similar to that in the training environments. Prior works (Hafner et al., 2019; Lee et al., 2020)

¹Department of Electrical and Computer Engineering, Boston University, Boston, MA 02215, USA. Correspondence to: Jiameng Fan <jmfan@bu.edu>, Wenchao Li <wenchao@bu.edu>.

that encode images into a low-dimensional latent space for RL typically rely on a reconstruction loss to learn representations that are sufficient to reconstruct the input images. While these approaches can learn representations that retain information in the visual observations, they do nothing to discard the irrelevant information.

We tackle this problem by learning robust representations for RL based on the multi-view information bottleneck (MIB) principle (Tishby et al., 2000; Federici et al., 2020). In the multi-view setting, we assume each view provides the same *task-relevant* information while all the information not shared by them is *task-irrelevant* (Zhang et al., 2018b). Data augmentation can be easily leveraged to generate such multi-view observations without requiring additional new data. Incorporating data augmentation into RL shows promising results for visual control tasks (Laskin et al., 2020; Lange et al., 2012) (Laskin et al., 2020; Lange et al., 2012). However, these methods rarely exploit the sequential aspect of RL that requires the learned representations to be predictive of the future. Instead of learning representations for each individual visual observation, ***we propose to learn a mapping from a sequence of observations to a sequence of representations given actions.*** Our approach exploits the fact that a robust RL agent, when operating under different views of the same environment, should exhibit similar behaviors. To enforce this similarity, ***the agent is optimized to learn robust representations that contain maximal task-relevant information and minimal task-irrelevant information.*** Concretely, we introduce a new MIB objective that maximizes the mutual information between sequences of observations and representations while reducing the task-irrelevant information identified through the multi-view observations. We incorporate this MIB objective into RL by optimize RL objectives on top of the learned encoder. We illustrate our proposed approach in Figure 1. Our contributions are summarized below.

- We propose DRIBO, a novel technique to learn robust representations in RL by identifying and discarding *task-irrelevant* information in the representations based on the multi-view information bottleneck principle.
- We leverage the sequential aspect of RL and define a new MIB objective that maximizes mutual information between sequences of representations and observations while disregarding *task-irrelevant* information without requiring reconstruction.
- Empirically, we show that our approach can (i) lead to better robustness against task-irrelevant distractors on the DeepMind Control Suite and (ii) significantly improve generalization on the Procgen benchmarks compared to current state-of-the-arts.

2. Related Work

Reconstruction-based Representation Learning. Early works trained autoencoders to learn sufficient representations to reconstruct raw observations first. Then, the RL agent was trained from the learned representations (Lange & Riedmiller, 2010; Lange et al., 2012). However, there is no guarantee that the agent will capture useful information for control. To address this problem, learning encoder and dynamics jointly has proved effective in learning task-oriented representations (Wahlström et al., 2015; Watter et al., 2015). More recently, Hafner et al. (2019; 2020) and Lee et al. (2020) learn a latent dynamics model and train RL agents with predictive latent representations. However, these approaches suffer from embedding all details into representations even when they are task-irrelevant. The reason is that improving reconstruction quality from representations to visual observations forces the representations to retain more details. Despite success on many benchmarks, task-irrelevant visual changes can affect the performance significantly (Zhang et al., 2018a). Experimentally, we show that our non-reconstructive approach, DRIBO, is substantially more robust against this type of visual changes than prior works. We also compare DRIBO with the recently introduced DBC (Zhang et al., 2021), which uses bisimulation metrics to learn representations in RL that contain only task-relevant information without requiring reconstruction.

Contrastive Representations Learning. Contrastive representation learning methods train an encoder that obeys similarity constraints in a dataset typically organized by similar and dissimilar pairs. The similar examples are typically obtained from nearby image patches (Oord et al., 2018; Hénaff et al., 2020) or through data augmentation (Chen et al., 2020). Contrastive models encourage similarity between features in representations using a variety of objectives. A scoring function that lower-bounds mutual information is one of the typical objects to be maximized (Belghazi et al., 2018; Oord et al., 2018; Hjelm et al., 2019; Poole et al., 2019). A number of works have applied the above ideas to RL settings. EMI (Kim et al., 2019) applies a Jensen-Shannon divergence-based lower bound on mutual information across subsequent frames as an exploration bonus. DRIML (Mazoure et al., 2020) uses an auxiliary contrastive objective to maximizes concordance between representations to increase predictive properties of the representations conditioned on actions. However, maximizing the lower-bound of mutual information retains all the information including the task-irrelevant information (Federici et al., 2020).

Multi-View Information Bottleneck (MIB). The multi-view setting relies on a basic assumption that each view provides the same task-relevant information while all the information not shared by the views are task-irrelevant (Zhao

et al., 2017). In classification, Federici et al. (2020) uses MIB by maximizing the mutual information between the representations of the two views while at the same time eliminating the label-irrelevant information. However, MIB cannot be directly used in RL settings due to the sequential nature of these decision making problems. Task-relevant information in RL is relevant because they influence not only current control and reward but also states and rewards in the future, which requires representations to be predictive of the future representations. Our work, DRIBO, learns robust representations with a predictive model to maximize the mutual information between sequences of representations and observations, while eliminating task-irrelevant information based on the information bottleneck principle. Learning a predictive model also adopts richer learning signals than those provided by individual observation and reward alone, which helps to reduce sample complexity. In addition to representation learning, MVRL (Li et al., 2019) uses the multi-view setting to form a generalization of partially observable Markov decision process which substantially reduces sample complexity by training RL agents on it.

3. Preliminaries

We denote Markov Decision Process (**MDP**) as \mathcal{M} , with state s , action a , and reward r . We denote a policy on \mathcal{M} as π . The agent’s goal is to learn a policy π that maximizes the cumulative rewards.

We consider *sufficiency* of representations from two perspectives. The first is the ability to derive optimal actions from the representations. The second is the ability to be predictive of future representations. We consider ideal latent representations as the states of some underlying MDP that only models task-relevant dynamics. DRL agents learn from visual observations by treating them as states. However, they rely on the heuristic of using consecutive observations to implicitly capture the predictive property. Besides, the visual observations contains far more excessive details than the underlying states.

Thus, instead of mapping a single-step observation to a state, we consider encoding a sequence of observations to a sequence of states. This also relaxes the requirement of using consecutive visual observations since the history of observations is considered. We define $\mathcal{S} \subseteq \mathbb{R}^d$ as the state-representation space. The visual observations are $o \in \mathcal{O}$. Let $a_{1:T}^*$ be the optimal action sequence for a sequence of observation $o_{1:T}$, where T is the length. We assume that $o_{1:T}$ contains enough information to obtain $a_{1:T}^*$ which maximizes the cumulative rewards.

With the above assumption, we define a piece of information as *task-relevant* if it is *minimally sufficient* to derive $a_{1:T}^*$. In contrast, *task-irrelevant* information does not contribute

to the choice of $a_{1:T}^*$. We first consider sufficient representations that are discriminative enough to obtain $a_{1:T}^*$. This property can be quantified by the amount of mutual information between $o_{1:T}$ and $a_{1:T}^*$ and mutual information between $s_{1:T}$ and $a_{1:T}^*$.

Definition 1. A sequence of representations $s_{1:T}$ of $o_{1:T}$ is *sufficient* for RL iff $I(o_{1:T}; a_{1:T}^*) = I(s_{1:T}; a_{1:T}^*)$.

RL agents that have access to a sufficient representation s_t at timestep t must be able to generate a_t^* as if it has access to the original observations. This can be better understood by subdividing $I(o_{1:T}; s_{1:T})$ into two components using the chain rule of mutual information:

$$I(o_{1:T}; s_{1:T}) = I(o_{1:T}; s_{1:T}|a_{1:T}^*) + I(s_{1:T}; a_{1:T}^*) \quad (1)$$

Conditional mutual information $I(o_{1:T}; s_{1:T}|a_{1:T}^*)$ quantifies the information in $s_{1:T}$ that is *task-irrelevant*. $I(s_{1:T}; a_{1:T}^*)$ quantifies *task-relevant* information that is accessible from the representation. Note that the last term is independent of the representation as long as s_t is sufficient for a_t^* (see Definition 1). Thus, a representation contains minimal task-irrelevant information whenever $I(o_{1:T}; s_{1:T}|a_{1:T}^*)$ is minimized. To obtain the sufficiency, we can maximize the mutual information $I(o_{1:T}; s_{1:T})$. With the information bottleneck principle, we can construct an objective to maximize $I(o_{1:T}; s_{1:T})$ while minimizing $I(o_{1:T}; s_{1:T}|a_{1:T}^*)$ to reduce task-irrelevant information.

However, minimizing $I(o_{1:T}; s_{1:T}|a_{1:T}^*)$ can be done directly only in supervised settings where $a_{1:T}^*$ are observed. In addition, the mutual information between sequences poses challenges for estimation. While MIB can reduce task-irrelevant information in the representations in an unsupervised settings (Federici et al., 2020), the strategy only considers a single observation and its representation. MIB does not guarantee that the learned representations retain the important sequential structure for RL. In the next section, we describe how we extend MIB to RL settings.

4. DRIBO

DRIBO learns robust representations that are predictive of future representations while discarding task-irrelevant information for control. To learn such representations, we construct a new MIB objective that (i) maximizes the mutual information between sequences of observations and representations, $I(s_{1:T}; o_{1:T}|a_{1:T})$ and (ii) quantifies and reduces task-irrelevant information in the representations based on the multi-view setting.

4.1. Mutual Information Maximization

To generalize the mutual information between sequences of observations and representations given any action sequences, we consider maximizing the conditional mutual

information $I(s_{1:T}; o_{1:T} | a_{1:T})$. The observations are temporally evolved in the environment by executing the conditioned actions. This conditional mutual information not only estimates the sufficiency of the representations but also maintains the sequential structure of RL problems.

However, the large dimension of the sequential data makes it challenging to estimate the mutual information. We first factorize the mutual information between two sequential data to the mutual information at each timestep.

Theorem 1. *Let $o_{1:T}$ be the observation sequence obtained by executing action sequence $a_{1:T}$. Let $s_{1:T}$ be a sequence of sufficient representations for $o_{1:T}$.*

$$I(s_{1:T}; o_{1:T} | a_{1:T}) \geq \sum_{t=1}^T I(s_t; o_t | s_{t-1}, a_{t-1}) \quad (2)$$

Proof. Let $H(\cdot)$ be the entropy of a random variable, and X and Y be two random variables. The mutual information between them can be expressed as $I(X; Y) = H(X) - H(X|Y)$. We apply the chain rule for entropy $H(X_1, X_2, \dots, X_n) = \sum_{i=1}^n H(X_i | X_{i-1}, \dots, X_1)$ and nonnegativity of mutual information in the proof. The last steps use Markov property of state transitions.

$$\begin{aligned} & I(s_{1:T}; o_{1:T} | a_{1:T}) \\ &= H(s_{1:T} | a_{1:T}) - H(s_{1:T} | o_{1:T}, a_{1:T}) \\ &= \sum_t (H(s_t | a_{1:T}, s_{1:t-1}) - H(s_t | a_{1:T}, o_{1:T}, s_{1:t-1})) \\ &= \sum_t I(s_t; o_{1:T} | a_{1:T}, s_{1:t-1}) \\ &= \sum_t (H(o_{1:T} | a_{1:T}, s_{1:t-1}) - H(o_{1:T} | s_t, a_{1:T}, s_{1:t-1})) \\ &= \sum_t \sum_{\tau} (H(o_{\tau} | a_{1:T}, s_{1:t-1}, o_{1:\tau-1}) \\ &\quad - H(o_{\tau} | s_t, a_{1:T}, s_{1:t-1}, o_{1:\tau-1})) \\ &= \sum_t \sum_{\tau} I(s_t; o_{\tau} | a_{1:T}, s_{1:t-1}, o_{1:\tau-1}) \\ &\geq \sum_t I(s_t; o_t | a_{1:T}, s_{1:t-1}, o_{1:t-1}) \\ &= \sum_t I(s_t; o_t | s_{t-1}, a_{t-1}) \end{aligned}$$

□

With Theorem 1, we show that the sum of mutual information $I(s_t; o_t | s_{t-1}, a_{t-1})$ over timesteps is a lower bound of the mutual information $I(s_{1:T}; o_{1:T} | a_{1:T})$. Even when the representations $s_{1:T}$ are not sufficient, maximizing $I(s_t; o_t | s_{t-1}, a_{t-1})$ encodes more details into s_t which will make it sufficient and satisfy Equation 2. The factorized mutual information is conditioned on the representation and the action at $t-1$, which explicitly retains the predictive information for future representations.

4.2. Multi-View Setting

To learn sufficient representations with minimal task-irrelevant information, we consider a multi-view setting to identify the task-irrelevant information without supervision. Consider $o_t^{(1)}$ and $o_t^{(2)}$ to be two visual images of the control scenario from different viewpoints. Assuming that the optimal control a_t^* can be clearly derived from both $o_t^{(1)}$ and $o_t^{(2)}$ conditioned on the representation and action at $t-1$. Then, any representation s_t containing all information accessible from both views and being predictive of future representations would contain the sufficient task-relevant information. Furthermore, if s_t captures only the details that are visible from both observations, it would eliminate the view-specific details and reduce the sensitivity of the representation to view-changes.

A sufficient representation in RL maintains all information which is shared by mutually redundant observations $o_t^{(1)}$ and $o_t^{(2)}$. We refer to Appendix A for sufficiency condition of representations and mutually redundancy condition between $o_t^{(1)}$ and $o_t^{(2)}$. Intuitively, with the mutual redundancy condition, any representation which contains all information shared by both views is as task-relevant as the joint observation. By factorizing the mutual information between $s_t^{(1)}$ and $o_t^{(1)}$ as in Equation 1, we can identify two components:

$$\begin{aligned} & I(s_t^{(1)}; o_t^{(1)} | s_{t-1}^{(1)}, a_{t-1}) \\ &= I(s_t^{(1)}; o_t^{(1)} | s_{t-1}^{(1)}, a_{t-1}, o_t^{(2)}) + I(o_t^{(2)}; s_t^{(1)} | s_{t-1}^{(1)}, a_{t-1}) \end{aligned} \quad (3)$$

Here, $s_{t-1}^{(1)}$ is a representation of visual observation $o_{t-1}^{(1)}$. Since we assume mutual redundancy between the two views, the information shared between $o_t^{(1)}$ and $s_t^{(1)}$ conditioned on $o_t^{(2)}$ must be irrelevant to the task, which can be quantified as $I(s_t^{(1)}; o_t^{(1)} | s_{t-1}^{(1)}, a_{t-1}, o_t^{(2)})$ (first term in Equation 3). Then, $I(o_t^{(2)}; s_t^{(1)} | s_{t-1}^{(1)}, a_{t-1})$ has to be maximal if the representation is sufficient. The formal description for the above statement can be found in Appendix A.

The less the two views have in common, the less task-irrelevant information can be encoded into the representations without violating sufficiency, and consequently, the less sensitive the resulting representation to task-irrelevant nuisances. In the extreme, we can show that $s_t^{(1)}$ is the underlying states of MDP if $o_t^{(1)}$ and $o_t^{(2)}$ share only task-relevant information. With Equation 2 and 3, we have the multi-view loss \mathcal{L}_{MV} , which maintains the temporally evolving information of the underlying dynamics.

$$\begin{aligned} \mathcal{L}_{\text{MV}} = & - \sum_t (I(s_t^{(1)}; o_t^{(1)} | s_{t-1}^{(1)}, a_{t-1}, o_t^{(2)}) \\ & + I(o_t^{(2)}; s_t^{(1)} | s_{t-1}^{(1)}, a_{t-1})) \end{aligned}$$

The above loss extends MIB to RL and maximizing it learns

representations that are sufficient and predictive of future representations. The multi-view observations can be trivially obtained with random data augmentation techniques so that each view is augmented differently.

4.3. DRIBO Loss Function

In Section 4.2, we show how to factorize the mutual information between sequences of observations and representations into mutual information at each timestep. This enables us to obtain sufficient representations by maximizing the mutual information between $s_t^{(1)}$ and $o_t^{(1)}$ while discarding task-irrelevant information by reducing $I(s_t^{(1)}; o_t^{(1)} | s_{t-1}^{(1)}, a_{t-1}, o_t^{(2)})$. The predictive properties are ensured by conditioning the mutual information on the previous timestep representation and action. With the information bottleneck principle, we can construct a relaxed Lagrangian loss to obtain a sufficient representation $s_t^{(1)}$ for $o_t^{(1)}$ with minimal task-irrelevant information:

$$\begin{aligned} \mathcal{L}_1(\theta; \lambda_1) = & I_\theta(s_t^{(1)}; o_t^{(1)} | s_{t-1}^{(1)}, a_{t-1}, o_t^{(2)}) \\ & - \lambda_1 I_\theta(o_t^{(2)}; s_t^{(1)} | s_{t-1}^{(1)}, a_{t-1}) \end{aligned} \quad (4)$$

where θ denotes the parameters of the encoder $p_\theta(s_t^{(1)} | o_t^{(1)}, s_{t-1}, a_{t-1})$, and λ_1 is the Lagrangian multiplier. Symmetrically, we define a loss \mathcal{L}_2 to learn a sufficient representation $s_t^{(2)}$ for $o_t^{(2)}$ with minimal task-irrelevant information:

$$\begin{aligned} \mathcal{L}_2(\theta; \lambda_2) = & I_\theta(s_t^{(2)}; o_t^{(2)} | s_{t-1}^{(2)}, a_{t-1}, o_t^{(1)}) \\ & - \lambda_2 I_\theta(o_t^{(1)}; s_t^{(2)} | s_{t-1}^{(2)}, a_{t-1}) \end{aligned} \quad (5)$$

By re-parameterizing the Lagrangian multipliers, the average of two loss functions \mathcal{L}_1 and \mathcal{L}_2 from two views at timestep t can be upper bounded as follows:

$$\begin{aligned} \mathcal{L}_t(\theta; \beta) = & -I_\theta(s_t^{(1)}; s_t^{(2)} | s_{t-1}, a_{t-1}) + \\ & \beta D_{\text{SKL}}(p_\theta(s_t^{(1)} | o_t^{(1)}, s_{t-1}^{(1)}, a_{t-1}) || p_\theta(s_t^{(2)} | o_t^{(2)}, s_{t-1}^{(2)}, a_{t-1})) \end{aligned} \quad (6)$$

where s_{t-1} is a sufficient representation, D_{SKL} represents the symmetrized KL divergence obtained by averaging the expected values of $D_{\text{KL}}(p_\theta(s_t^{(1)} | o_t^{(1)}, s_{t-1}^{(1)}, a_{t-1}) || p_\theta(s_t^{(2)} | o_t^{(2)}, s_{t-1}^{(2)}, a_{t-1}))$, $D_{\text{KL}}(p_\theta(s_t^{(2)} | o_t^{(2)}, s_{t-1}^{(2)}, a_{t-1}) || p_\theta(s_t^{(1)} | o_t^{(1)}, s_{t-1}^{(1)}, a_{t-1}))$, and the coefficient β represent the trade-off between sufficiency and sensitivity to task-irrelevant information. β is a hyper-parameter in this work.

To generalize the above loss to sequential data in RL, we apply Theorem 1 to obtain the DRIBO loss:

$$\mathcal{L}_{\text{DRIBO}} = \frac{1}{T} \sum_{t=1}^T \mathcal{L}_t(\theta; \beta) \quad (7)$$

Algorithm 1 DRIBO Loss

input : Batch \mathcal{B} sampled from replay buffer storing N sequential observations and actions with length T .

- 1: Apply random augmentation transformations on \mathcal{B} to obtain multi-view batches $\mathcal{B}^{(1)}$ and $\mathcal{B}^{(2)}$.
- 2: **for** $i, (o_{1:T}^{(1)}, o_{1:T}^{(2)}, a_{1:T})$ in enumerate $(\mathcal{B}^{(1)}, \mathcal{B}^{(2)})$ **do**
- 3: **for** $t = 1$ to T **do**
- 4: We substitute s_{t-1} with $s_{t-1}^{(1)}$ and $s_{t-1}^{(2)}$ given the multi-view assumption. {Analysis in Appendix B}
- 5: $s_t^{(1)} \sim p_\theta(s_t^{(1)} | o_t^{(1)}, s_{t-1}^{(1)}, a_{t-1})$
- 6: $s_t^{(2)} \sim p_\theta(s_t^{(2)} | o_t^{(2)}, s_{t-1}^{(2)}, a_{t-1})$
- 7: $(s^{(1),t+T(i-1)}, s^{(2),t+T(i-1)}) \leftarrow (s_t^{(1)}, s_t^{(2)})$
- 8: **end for**
- 9: $\mathcal{L}_{\text{SKL}}^i = \frac{1}{T} \sum_{t=1}^T D_{\text{DKL}}(p_\theta(s_t^{(1)}) || p_\theta(s_t^{(2)}))$
- 10: **end for**
- 11: **return** $-\hat{I}_\psi(\{(s^{(1),i}, s^{(2),i})\}_{i=1}^{T*N}) + \frac{\beta}{N} \sum_{i=1}^N \mathcal{L}_{\text{SKL}}^i$

We summarize the batch-based computation of the loss function in Algorithm 1. We sample $s_t^{(1)}$ and $s_t^{(2)}$ from $p_\theta(s_t^{(1)} | o_t^{(1)}, s_{t-1}^{(1)}, a_{t-1})$ and $p_\theta(s_t^{(2)} | o_t^{(2)}, s_{t-1}^{(2)}, a_{t-1})$ respectively. Though first term in Equation 6 is conditioned on s_{t-1} , we prove that the sampling process does not affect its effectiveness based on the multi-view assumption in Appendix B. The symmetrized KL divergence term can be computed from the probability density of $s_t^{(1)}$ and $s_t^{(2)}$ estimated by the encoder. The mutual information between the two representations $I_\theta(s_t^{(1)}; s_t^{(2)} | s_{t-1}, a_{t-1})$ can be maximized by using any sample-based differentiable mutual information lower bound $\hat{I}_\psi(s_t^{(1)}, s_t^{(2)})$, where ψ represents the learnable parameters. We use InfoNCE (Oord et al., 2018) to estimate mutual information since the multi-view setting provides a large number of negative examples. The positive pairs are the representations $(s_t^{(1)}, s_t^{(2)})$ of the multi-view observations generated from the same observation. The remaining pairs of representations within the same batch are used as negative pairs. The full derivation for the DRIBO loss function can be found in Appendix B.

4.4. Encoder Architecture

The encoder $p_\theta(s_t | o_t, s_{t-1}, a_{t-1})$ approximates representation posteriors from current observation, the previous timestep representation and action. The posteriors can also be seen as a reparameterization of $p_\theta(s_{1:T} | o_{1:T}, a_{1:T}) = \prod_t p_\theta(s_t | o_t, s_{t-1}, a_{t-1})$, which explicitly maintain the inherent sequential structure of RL.

We implement the encoder as a recurrent space model (RSSM (Hafner et al., 2019)) with a convolutional neural network (CNN) applied to the visual observations. RSSM is a latent dynamics model with an expressive recurrent neural network to perform accurate long-term prediction. We split

the representation s_t into a stochastic part z_t and a deterministic part h_t , where $s_t = (z_t, h_t)$. The generative and inference models of RSSM are defined as:

Deterministic state transition: $h_t = f(h_{t-1}, z_{t-1}, a_{t-1})$

Stochastic state transition: $z_t = p(z_t | h_t)$

Observation model: $o_t = p(o_t | h_t, z_t)$

where $f(h_{t-1}, z_{t-1}, a_{t-1})$ is implemented as a recurrent neural network (RNN) that carries the dependency on the stochastic and deterministic parts at the previous timestep. Then, we obtain the representation with the encoder $p_\theta((s_{1:T} | o_{1:T}, a_{1:T}) = \prod_t p_\theta(s_t | o_t, h_t)$, where h_t retains information from $s_{t-1} = (z_{t-1}, h_{t-1})$ and a_{t-1} . The encoder architecture based on the RSSM model encourages the representations to be predictive of future states, which aligns with the key property of DRIBO.

4.5. Incorporating DRIBO in RL

We simultaneously train our representation learning models with the RL agent by adding $\mathcal{L}_{\text{DRIBO}}$ (Algorithm 1) as an auxiliary objective during training. The multi-view observations required by DRIBO can be trivially obtained using the same experience replay of RL agents with data augmentation. The policy and (or) value function in RL will directly take the representation s_t of the original visual observation o_t to allow the models in RL to backprop to our encoder. This further improves the performance by accommodating the learned representations with policy/value function. As a result, DRIBO encourages the agent to learn the underlying task-relevant dynamics of the environments while being robust against visual changes that are task-irrelevant.

We demonstrate the effectiveness of DRIBO by building the agents on top of SAC (Haarnoja et al., 2018) and PPO (Schulman et al., 2017) in Section 5.1 and Section 5.2 respectively. More details can be found in Appendix C.

5. Experiment

We experimentally evaluate DRIBO on a variety of visual control tasks. We designed the experiments to compare DRIBO to current best methods in the literature on: (i) the effectiveness of solving visual control tasks, (ii) their robustness against task-irrelevant distractors, and (iii) the ability to generalize to unseen environments.

For effectiveness, we demonstrate performance on the Deep-Mind Control Suite with no distractors (DMC (Tassa et al., 2018)). The DMC suite provides qualitatively different visual control challenges. For robustness, we investigate whether our DRIBO agent can ignore high-dimensional visual distractors that are task-irrelevant in the DMC environments when the backgrounds are replaced with natural videos from

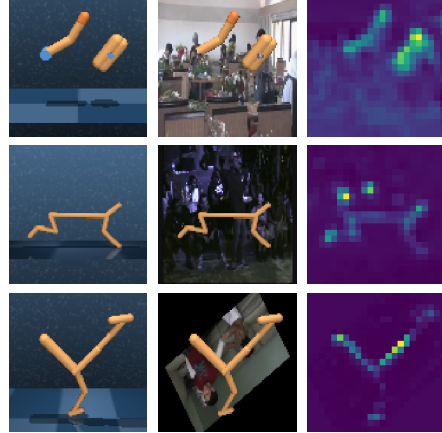


Figure 2: The left images are observations in DMC in the clean setting. The center images are observations in DMC using natural videos as background. The right images are the spatial attention maps of the encoder for the center images.

the Kinetics dataset (Kay et al., 2017). For generalization, we present results on Procgen (Cobbe et al., 2020) which provides different levels of the same game to test how well agents generalize to unseen levels. Since DRIBO does not assume that observation at each timestep provides full observability of the underlying dynamics, we use single-step observations to train the DRIBO representations. By contrast, current SOTA approaches require the use of consecutive observations¹ to capture predictive property implicitly.

For the DMC suite, all agents are built on top of SAC, an off-policy RL algorithm. For the Procgen suite, we augment PPO, an on-policy RL baseline on Procgen, with DRIBO. Implementation details are given in Appendix C.

5.1. Effectiveness and Robustness

First, we focus on studying the effectiveness and robustness of DRIBO trained agents. We evaluate our approach on DMC under ‘clean’ settings (without distractors), as well as much more difficult settings with distractors.

We compare DRIBO against several baselines. The first is RAD (Laskin et al., 2020), a recent method that uses augmented data to train pixel-based policy and achieved state-of-art performance on DMC. The second is SLAC (Lee et al., 2020), a SOTA representation learning method for RL that learns a dynamics model with a reconstruction loss. Finally, we compare with DBC (Zhang et al., 2021) which is the most similar work to ours. DBC learns an invariant representation based on bisimulation metrics without requiring reconstruction. For RAD and DRIBO, we apply *crop+random grayscale* to obtain augmented data and multi-view

¹ All methods compared in our experiments stacks 3 consecutive observations while DRIBO does not use frame stack.

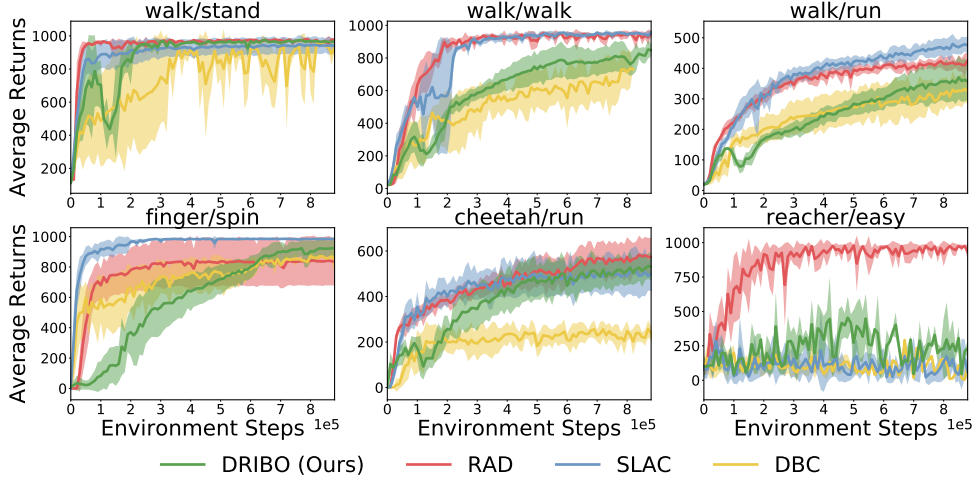


Figure 3: Average returns on DMC tasks over 5 seeds with mean and one standard error shaded in the clean setting.

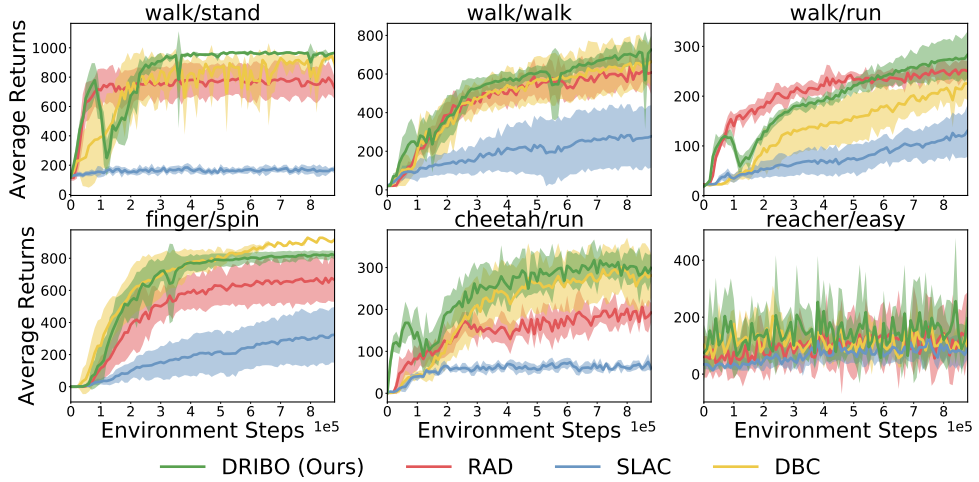


Figure 4: Average returns on DMC tasks over 5 seeds with mean and one standard error shaded in the natural video setting.

observations across different settings.

Clean Setting. For clean setting, the pixel observations have simple backgrounds as shown in Figure 2 (left column). Figure 3 shows that RAD and SLAC generally perform the best, whereas DRIBO outperforms DBC and matches SOTA in some of the environments. However, since the testing and training environments are identical, the RL agents may overfit to the training environments.

Natural Video Setting. Next, we introduce high-dimensional visual distractors by using natural videos from the Kinetics dataset (Kay et al., 2017) as new backgrounds (Zhang et al., 2018a) (Figure 2: middle column). To avoid the issue of overfitting, we use different natural videos to replace the background in training and testing.

In Figure 2, spatial attention maps (Zagoruyko & Komodakis, 2017) of the trained DRIBO encoder demonstrate

that DRIBO trains agents to focus on the robot body while ignoring irrelevant scene details in the background. Figure 4 shows that DRIBO performs substantially better than RAD and SLAC which do not discard task-irrelevant information explicitly. Compared with DBC, a recent state-of-art method for learning representations that are invariant to task-irrelevant information, DRIBO either outperforms or matches its performance.

Visualizing Learned Representations. We visualize the representations learned with the DRIBO loss function in Algorithm 1 with t-SNE (Van der Maaten & Hinton, 2008). Figure 5 shows that even when the background looks drastically different, DRIBO learns to disregard irrelevant information and maps observations with similar robot configurations to the neighborhoods of one another. The color code represents values of reward for each representation. We observe that neighboring representations share close reward

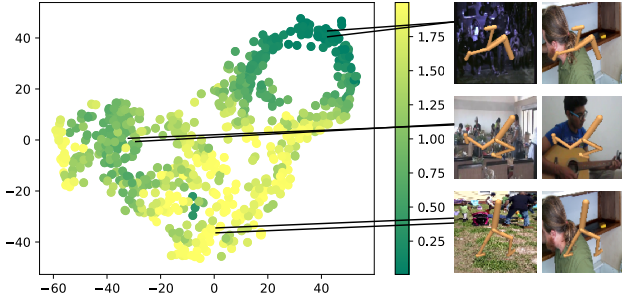


Figure 5: t-SNE of latent spaces learned with DRIBO. We color-code the embedded points with reward values (high value yellow, lower value green). DRIBO learns representations that are neighboring in the embedding space with similar reward values, which are the direct task-relevant signals from the environments. This property also holds even if the backgrounds are drastically different (see right visual images). The solid lines refer to the corresponding embedded points for each observation.

values. The rewards can be viewed as task-relevant signals provided by the environments.

5.2. Generalization

Though the natural video setting of DMC is suitable for benchmarking robustness to high-dimensional visual distractors, the task-relevant information and the task difficulties are unchanged. For this reason, we use the ProcGen suite (Cobbe et al., 2020) to investigate the generalization capabilities of DRIBO. Our training setting consists of fixing the first 200 levels of a given Procgen game to train agents and then using the remaining levels as unseen levels to evaluate generalization performance. Unseen levels typically have different backgrounds or different layouts, which are easy for humans to adapt but challenging for RL agents.

We compare DRIBO with recent methods that incorporate data augmentation. All approaches are implemented based on PPO. RAD (Laskin et al., 2020) feeds augmented observation directly into RL policy and value function to enrich the diversity of training samples. DrAC (Raileanu et al., 2020) applies two regularization terms for policy and value function using augmented data. UCB-DrAC is built on top of DrAC, which automatically selects the best type of data augmentation for DrAC. For RAD and DrAC, we use the best reported augmentation types for different environments. DRIBO select the same augmentation types except for a few games. The details about data augmentation types used in the Procgen environments can be found in Appendix C.

Results in Table 1 show that DRIBO attains higher averaged testing returns compared to the PPO baseline and augmentation-based RL baselines. A few environments,

in which our approach does not outperform others, share the commonality that task-relevant layouts remain static throughout the same run of the game. Since the current version of DRIBO only considers the mutual information between the complete input and the encoder output (global MI (Hjelm et al., 2019)), it may fail to capture local features. The representations for a sequence of observations within the same run of the game are globally negative pairs but locally positive pairs. Thus, DRIBO performance can be further improved by considering local features (positions of the layouts) shared between representations as positive pairs in mutual information maximization.

Table 1: Procgen returns on test levels after training on 25M environment steps. The mean and standard deviation are computed over 10 runs.

Env	PPO	RAD	DrAC	UCB-DrAC	DRIBO
BigFish	4.0 ± 1.2	9.9 ± 1.7	8.7 ± 1.4	9.7 ± 1.0	10.9 ± 1.6
StarPilot	24.7 ± 3.4	33.4 ± 5.1	29.5 ± 5.4	30.2 ± 2.8	36.5 ± 3.0
FruitBot	26.7 ± 0.8	27.3 ± 1.8	28.2 ± 0.8	28.3 ± 0.9	30.8 ± 0.8
BossFight	7.7 ± 1.0	7.9 ± 0.6	7.5 ± 0.8	8.3 ± 0.8	12.0 ± 0.5
Ninja	5.9 ± 0.7	6.9 ± 0.8	7.0 ± 0.4	6.9 ± 0.6	9.7 ± 0.7
Plunder	5.0 ± 0.5	8.5 ± 1.2	9.5 ± 1.0	8.9 ± 1.0	5.8 ± 1.0
CaveFlyer	5.1 ± 0.9	5.1 ± 0.6	6.3 ± 0.8	5.3 ± 0.9	7.5 ± 1.0
CoinRun	8.5 ± 0.5	9.0 ± 0.8	8.8 ± 0.2	8.5 ± 0.6	9.2 ± 0.7
Jumper	5.8 ± 0.5	6.5 ± 0.6	6.6 ± 0.4	6.4 ± 0.6	8.4 ± 1.6
Chaser	5.0 ± 0.8	5.9 ± 1.0	5.7 ± 0.6	6.7 ± 0.6	4.8 ± 0.8
Climber	5.7 ± 0.8	6.9 ± 0.8	7.1 ± 0.7	6.5 ± 0.8	8.1 ± 1.6
DodgeBall	11.7 ± 0.3	2.8 ± 0.7	4.3 ± 0.8	4.7 ± 0.7	3.8 ± 0.9
Heist	2.4 ± 0.5	4.1 ± 1.0	4.0 ± 0.8	4.0 ± 0.7	7.7 ± 1.6
Leaper	4.9 ± 0.7	4.3 ± 1.0	5.3 ± 1.1	5.0 ± 0.3	5.3 ± 1.5
Maze	5.7 ± 0.6	6.1 ± 1.0	6.6 ± 0.8	6.3 ± 0.6	8.5 ± 1.6
Miner	8.5 ± 0.5	9.4 ± 1.2	9.8 ± 0.6	9.7 ± 0.7	9.8 ± 0.9
Norm.score	1.0	1.1	1.1	1.1	1.3

6. Conclusion

In this paper, we introduce a novel robust representation learning approach in RL based on the multi-view information bottleneck principle. Visual observations are encoded into representations that are robust against different task-irrelevant details and predictive of the future, a property central to the sequential aspect of RL. Our experimental results show that 1) DRIBO learns representations that are robust against task-irrelevant distractions and boosts training performance when complex visual distractors are introduced, 2) exploiting the sequential aspect of RL helps to learn more effective representations and 3) DRIBO improves generalization performance compared to well-established baselines on the large-scale Procgen benchmarks.

Future Work. We plan to explore the direction of incorporating knowledge about locality in the observations into DRIBO. In addition, our latent dynamics RSSM model was only used for training our encoder. We plan to augment model-based RL algorithms with DRIBO learned RSSM model to train RL agents in the future.

References

Belghazi, M. I., Baratin, A., Rajeshwar, S., Ozair, S., Bengio, Y., Courville, A., and Hjelm, D. Mutual information neural estimation. In *International Conference on Machine Learning*, pp. 531–540. PMLR, 2018.

Chen, T., Kornblith, S., Norouzi, M., and Hinton, G. A simple framework for contrastive learning of visual representations. In *International conference on machine learning*, pp. 1597–1607. PMLR, 2020.

Cobbe, K., Klimov, O., Hesse, C., Kim, T., and Schulman, J. Quantifying generalization in reinforcement learning. In *International Conference on Machine Learning*, pp. 1282–1289. PMLR, 2019.

Cobbe, K., Hesse, C., Hilton, J., and Schulman, J. Leveraging procedural generation to benchmark reinforcement learning. In *International Conference on Machine Learning*. PMLR, 2020.

Farebrother, J., Machado, M. C., and Bowling, M. Generalization and regularization in dqn. *arXiv preprint arXiv:1810.00123*, 2018.

Federici, M., Dutta, A., Forré, P., Kushman, N., and Akata, Z. Learning robust representations via multi-view information bottleneck. *International Conference on Learning Representation*, 2020.

Haarnoja, T., Zhou, A., Abbeel, P., and Levine, S. Soft actor-critic: Off-policy maximum entropy deep reinforcement learning with a stochastic actor. In *International Conference on Machine Learning*, pp. 1861–1870. PMLR, 2018.

Hafner, D., Lillicrap, T., Fischer, I., Villegas, R., Ha, D., Lee, H., and Davidson, J. Learning latent dynamics for planning from pixels. In *International Conference on Machine Learning*, pp. 2555–2565. PMLR, 2019.

Hafner, D., Lillicrap, T., Ba, J., and Norouzi, M. Dream to control: Learning behaviors by latent imagination. *International Conference on Learning Representation*, 2020.

Hénaff, O. J., Srinivas, A., De Fauw, J., Razavi, A., Doersch, C., Eslami, S., and van den Oord, A. Data-efficient image recognition with contrastive predictive coding. In *International Conference on Machine Learning*, pp. 4182–4192. PMLR, 2020.

Hjelm, R. D., Fedorov, A., Lavoie-Marchildon, S., Grewal, K., Bachman, P., Trischler, A., and Bengio, Y. Learning deep representations by mutual information estimation and maximization. *International Conference on Learning Representation*, 2019.

Kay, W., Carreira, J., Simonyan, K., Zhang, B., Hillier, C., Vijayanarasimhan, S., Viola, F., Green, T., Back, T., Natsev, P., et al. The kinetics human action video dataset. *arXiv preprint arXiv:1705.06950*, 2017.

Kim, H., Kim, J., Jeong, Y., Levine, S., and Song, H. O. Emi: Exploration with mutual information. In *International Conference on Machine Learning*, pp. 3360–3369, 2019.

Lange, S. and Riedmiller, M. Deep auto-encoder neural networks in reinforcement learning. In *The 2010 International Joint Conference on Neural Networks (IJCNN)*, pp. 1–8. IEEE, 2010.

Lange, S., Riedmiller, M., and Voigtlander, A. Autonomous reinforcement learning on raw visual input data in a real world application. In *The 2012 international joint conference on neural networks (IJCNN)*, pp. 1–8. IEEE, 2012.

Laskin, M., Lee, K., Stooke, A., Pinto, L., Abbeel, P., and Srinivas, A. Reinforcement learning with augmented data. *Advances in Neural Information Processing Systems*, 33, 2020.

Lee, A., Nagabandi, A., Abbeel, P., and Levine, S. Stochastic latent actor-critic: Deep reinforcement learning with a latent variable model. *Advances in Neural Information Processing Systems*, 33, 2020.

Li, M., Wu, L., Jun, W., and Ammar, H. B. Multi-view reinforcement learning. In *Advances in neural information processing systems*, pp. 1420–1431, 2019.

Mazoure, B., Tachet des Combes, R., DOAN, T. L., Bachman, P., and Hjelm, R. D. Deep reinforcement and info-max learning. *Advances in Neural Information Processing Systems*, 33, 2020.

Oord, A. v. d., Li, Y., and Vinyals, O. Representation learning with contrastive predictive coding. *arXiv preprint arXiv:1807.03748*, 2018.

Poole, B., Ozair, S., Van Den Oord, A., Alemi, A., and Tucker, G. On variational bounds of mutual information. In *International Conference on Machine Learning*, pp. 5171–5180. PMLR, 2019.

Raileanu, R., Goldstein, M., Yarats, D., Kostrikov, I., and Fergus, R. Automatic data augmentation for generalization in deep reinforcement learning. *arXiv preprint arXiv:2006.12862*, 2020.

Schulman, J., Wolski, F., Dhariwal, P., Radford, A., and Klimov, O. Proximal policy optimization algorithms. *arXiv preprint arXiv:1707.06347*, 2017.

Tassa, Y., Doron, Y., Muldal, A., Erez, T., Li, Y., Casas, D. d. L., Budden, D., Abdolmaleki, A., Merel, J., Lefrancq,

A., et al. Deepmind control suite. *arXiv preprint arXiv:1801.00690*, 2018.

Tishby, N., Pereira, F. C., and Bialek, W. The information bottleneck method. *arXiv preprint physics/0004057*, 2000.

Van der Maaten, L. and Hinton, G. Visualizing data using t-sne. *Journal of machine learning research*, 9(11), 2008.

Wahlström, N., Schön, T. B., and Desienroth, M. P. From pixels to torques: Policy learning with deep dynamical models. In *Deep Learning Workshop at the 32nd International Conference on Machine Learning (ICML 2015), July 10-11, Lille, France*, 2015.

Watter, M., Springenberg, J. T., Boedecker, J., and Riedmiller, M. Embed to control: a locally linear latent dynamics model for control from raw images. In *Proceedings of the 28th International Conference on Neural Information Processing Systems-Volume 2*, pp. 2746–2754, 2015.

Yu, W., Liu, C. K., and Turk, G. Policy transfer with strategy optimization. In *International Conference on Learning Representations*, 2019.

Zagoruyko, S. and Komodakis, N. Paying more attention to attention: Improving the performance of convolutional neural networks via attention transfer. *International Conference on Learning Representation*, 2017.

Zhang, A., Wu, Y., and Pineau, J. Natural environment benchmarks for reinforcement learning. *arXiv preprint arXiv:1811.06032*, 2018a.

Zhang, A., McAllister, R., Calandra, R., Gal, Y., and Levine, S. Learning invariant representations for reinforcement learning without reconstruction. *International Conference on Learning Representation*, 2021.

Zhang, C., Vinyals, O., Munos, R., and Bengio, S. A study on overfitting in deep reinforcement learning. *arXiv preprint arXiv:1804.06893*, 2018b.

Zhao, J., Xie, X., Xu, X., and Sun, S. Multi-view learning overview: Recent progress and new challenges. *Information Fusion*, 38:43–54, 2017.

Appendix

A. Theorems and Proofs

In this section, we first list properties of the mutual information we used in our proof. For any random variables X, Y and Z .

(P.1) Positivity:

$$I(X; Y) \geq 0, I(X; Y|Z) \geq 0$$

(P.2) Chain rule:

$$I(XY; Z) = I(Y; Z) + I(X; Z|Y)$$

(P.3) Chain rule (Multivariate Mutual Information):

$$I(X; Y; Z) = I(Y; Z) - I(Y; Z|X)$$

(P.4) Entropy and Mutual Information:

$$I(X; Y) = H(X) - H(X|Y)$$

(P.5) Chain rule for Entropy:

$$H(X_1, X_2, \dots, X_n) = \sum_{i=1}^n H(X_i | X_{i-1}, \dots, X_1)$$

A.1. Theorem 1

Here, we relax the sufficiency condition in Theorem 1 and generalize the theorem to representations sampled from a encoder $p_\theta(s_{1:T} | o_{1:T}, a_{1:T})$.

Theorem A.1. *Let $o_{1:T}$ be the observation sequence obtained by executing action sequence $a_{1:T}$. Let $s_{1:T}$ be a sequence of representations for $o_{1:T}$ sampled from an encoder with a specific architecture, $p_\theta(s_{1:T} | o_{1:T}, a_{1:T})$.*

$$I(s_{1:T}; o_{1:T} | a_{1:T}) \geq \sum_{t=1}^T I(s_t; o_t | s_{t-1}, a_{t-1}) \quad (8)$$

Proof. We specify the property we used for each step of derivation. The last equality holds since $s_{1:t-1} \sim p_\theta(s_{1:t-1} | o_{1:t-1}, a_{1:t-1})$. All information contained in $o_{1:t-1}$ are observed by s_{t-1} with the factorized probability $p_\theta(s_{t-1} | o_{t-1}, s_{t-2}, a_{t-2})$. Then, s_{t-1} contain all the

information in $o_{1:t-1}$, $s_{1:t-2}$ and $a_{1:t-2}$.

$$\begin{aligned} & I(s_{1:T}; o_{1:T} | a_{1:T}) \\ & \stackrel{(P.4)}{=} H(s_{1:T} | a_{1:T}) - H(s_{1:T} | o_{1:T}, a_{1:T}) \\ & \stackrel{(P.5)}{=} \sum_t (H(s_t | a_{1:T}, s_{1:t-1}) - H(s_t | a_{1:T}, o_{1:T}, s_{1:t-1})) \\ & \stackrel{(P.4)}{=} \sum_t (H(o_{1:T} | a_{1:T}, s_{1:t-1}) - H(o_{1:T} | s_t, a_{1:T}, s_{1:t-1})) \\ & \stackrel{(P.5)}{=} \sum_t \sum_\tau (H(o_\tau | a_{1:T}, s_{1:t-1}, o_{1:\tau-1}) \\ & \quad - H(o_\tau | s_t, a_{1:T}, s_{1:t-1}, o_{1:\tau-1})) \\ & \stackrel{(P.4)}{=} \sum_t \sum_\tau I(s_t; o_\tau | a_{1:T}, s_{1:t-1}, o_{1:\tau-1}) \\ & \stackrel{(P.1)}{\geq} \sum_t I(s_t; o_t | a_{1:T}, s_{1:t-1}, o_{1:t-1}) \\ & = \sum_t I(s_t; o_t | s_{t-1}, a_{t-1}) \end{aligned}$$

With the above generalization, this lower bound holds for any representations sampled from $p_\theta(s_{1:T} | o_{1:T}, a_{1:T})$. As a result, \mathcal{L}_{MV} is a lower bound of $I(s_{1:T}; o_{1:T} | a_{1:T})$.

$$\begin{aligned} I(s_{1:T}^{(1)}; o_{1:T}^{(1)} | a_{1:T}) & \geq - \sum_t (I(s_t^{(1)}; o_t^{(1)} | s_{t-1}^{(1)}, a_{t-1}, o_t^{(2)}) \\ & \quad + I(o_t^{(2)}; s_t^{(1)} | s_{t-1}^{(1)}, a_{t-1})) \end{aligned}$$

□

A.2. Sufficient Representations in RL

In this section, we first present the sufficiency condition for sequential data. Then, we prove that if the sufficiency condition on the sequential data holds, then the sufficiency condition on each corresponding individual representation and observation holds as well.

Theorem A.2. *Let $o_{1:T}$ and $a_{1:T}^*$ be random variables with joint distribution $p(o_{1:T}, a_{1:T}^*)$. Let $s_{1:T}$ be the representation of $o_{1:T}$, then $s_{1:T}$ is sufficient for $a_{1:T}^*$ if and only if $I(o_{1:T}; a_{1:T}^*) = I(s_{1:T}; a_{1:T}^*)$. Also, s_t is a sufficient representation of o_t since $I(o_t; a_t^* | s_t, s_{t-1}, a_{t-1}) = 0$.*

Hypothesis:

(H.1) *$s_{1:T}$ is a sequence of sufficient representations for $o_{1:T}$:*

$$I(o_{1:T}; a_{1:T}^* | s_{1:T}) = 0$$

Proof.

$$\begin{aligned}
 & I(\mathbf{o}_{1:T}; \mathbf{a}_{1:T}^* | \mathbf{s}_{1:T}) \\
 \stackrel{\text{(P.3)}}{=} & I(\mathbf{o}_{1:T}; \mathbf{a}_{1:T}^*) - I(\mathbf{o}_{1:T}; \mathbf{a}_{1:T}^* | \mathbf{s}_{1:T}) \\
 \stackrel{\text{(P.3)}}{=} & I(\mathbf{o}_{1:T}; \mathbf{a}_{1:T}^*) - I(\mathbf{a}_{1:T}^*; \mathbf{s}_{1:T}) - I(\mathbf{a}_{1:T}^*; \mathbf{s}_{1:T} | \mathbf{o}_{1:T})
 \end{aligned}$$

With $\mathbf{s}_{1:T}$ as a representation of $\mathbf{o}_{1:T}$, we have $I(\mathbf{s}_{1:T}; \mathbf{a}_{1:T}^* | \mathbf{o}_{1:T}) = 0$. The reason is that $\mathbf{o}_{1:T}$ shares the same level of information as $\mathbf{a}_{1:T}^*$ and $\mathbf{s}_{1:T}$. Then,

$$I(\mathbf{o}_{1:T}; \mathbf{a}_{1:T}^* | \mathbf{s}_{1:T}) = I(\mathbf{o}_{1:T}; \mathbf{a}_{1:T}^*) - I(\mathbf{a}_{1:T}^*; \mathbf{s}_{1:T}) \quad (9)$$

So the sufficiency condition $I(\mathbf{o}_{1:T}; \mathbf{a}_{1:T}^* | \mathbf{s}_{1:T}) = 0$ holds if and only if $I(\mathbf{o}_{1:T}; \mathbf{a}_{1:T}^*) = I(\mathbf{a}_{1:T}^*; \mathbf{s}_{1:T})$.

We factorize the mutual information between sequential observations and optimal actions

$$\begin{aligned}
 & I(\mathbf{o}_{1:t}; \mathbf{a}_{1:t}^*) \\
 \stackrel{\text{(P.2)}}{=} & I(\mathbf{o}_t; \mathbf{a}_{1:t}^* | \mathbf{o}_{1:t-1}) + I(\mathbf{o}_{1:t-1}; \mathbf{a}_{1:t}^*) \\
 \stackrel{\text{(H.1)}}{=} & I(\mathbf{o}_t; \mathbf{a}_{1:t}^* | \mathbf{o}_{1:t-1}) + I(\mathbf{s}_{1:t-1}; \mathbf{a}_{1:t}^*) \\
 \\
 & I(\mathbf{s}_{1:t}; \mathbf{a}_{1:t}^*) \\
 \stackrel{\text{(P.2)}}{=} & I(\mathbf{s}_t; \mathbf{a}_{1:t}^* | \mathbf{s}_{1:t-1}) + I(\mathbf{s}_{1:t-1}; \mathbf{a}_{1:t}^*) \\
 \stackrel{\text{(H.1)}}{=} & I(\mathbf{s}_t; \mathbf{a}_{1:t}^* | \mathbf{s}_{1:t-1}) + I(\mathbf{o}_{1:t-1}; \mathbf{a}_{1:t}^*)
 \end{aligned}$$

Then we obtain the following relation:

$$I(\mathbf{o}_t; \mathbf{a}_{1:t}^* | \mathbf{o}_{1:t-1}) = I(\mathbf{s}_t; \mathbf{a}_{1:t}^* | \mathbf{s}_{1:t-1}) \quad (10)$$

We also have

$$\begin{aligned}
 & I(\mathbf{o}_t; \mathbf{a}_{1:t}^* | \mathbf{o}_{1:t-1}) \\
 \stackrel{\text{(P.2)}}{=} & I(\mathbf{o}_{1:t}; \mathbf{a}_{1:t}^*) - I(\mathbf{o}_{1:t-1}; \mathbf{a}_{1:t}^*) \\
 \stackrel{\text{(P.2)}}{=} & I(\mathbf{o}_{1:t-1}; \mathbf{a}_{1:t}^* | \mathbf{o}_t) + I(\mathbf{o}_t; \mathbf{a}_{1:t}^*) \\
 & - I(\mathbf{o}_{1:t-1}; \mathbf{a}_{1:t}^*) \\
 \stackrel{\text{(H.1)}}{=} & I(\mathbf{s}_{1:t-1}; \mathbf{a}_{1:t}^* | \mathbf{o}_t) + I(\mathbf{o}_t; \mathbf{a}_{1:t}^*) \\
 & - I(\mathbf{s}_{1:t-1}; \mathbf{a}_{1:t}^*) \\
 \stackrel{\text{(P.2)}}{=} & I(\mathbf{o}_t \mathbf{s}_{1:t-1}; \mathbf{a}_{1:t}^*) - I(\mathbf{s}_{1:t-1}; \mathbf{a}_{1:t}^*) \\
 \stackrel{\text{(P.2)}}{=} & I(\mathbf{o}_t; \mathbf{a}_{1:t}^* | \mathbf{s}_{1:t-1})
 \end{aligned}$$

$$\stackrel{\text{Equation 10}}{=} I(\mathbf{s}_t; \mathbf{a}_{1:t}^* | \mathbf{s}_{1:t-1})$$

$\xleftarrow{\text{(P.2)}}$

$$\begin{aligned}
 & I(\mathbf{o}_t; \mathbf{a}_t^* | \mathbf{a}_{1:t-1}^*, \mathbf{s}_{1:t-1}) + I(\mathbf{o}_t; \mathbf{a}_{1:t-1}^* | \mathbf{s}_{1:t-1}) \\
 = & I(\mathbf{s}_t; \mathbf{a}_t^* | \mathbf{a}_{1:t-1}^*, \mathbf{s}_{1:t-1}) + I(\mathbf{s}_t; \mathbf{a}_{1:t-1}^* | \mathbf{s}_{1:t-1})
 \end{aligned}$$

$\xleftarrow{\text{Equation 10}}$

$$I(\mathbf{o}_t; \mathbf{a}_t^* | \mathbf{a}_{1:t-1}^*, \mathbf{s}_{1:t-1}) = I(\mathbf{s}_t; \mathbf{a}_t^* | \mathbf{a}_{1:t-1}^*, \mathbf{s}_{1:t-1})$$

$\xleftarrow{\text{Equation 9}}$

$$I(\mathbf{o}_t, \mathbf{a}_t^* | \mathbf{s}_t, \mathbf{s}_{1:t-1}, \mathbf{a}_{1:t-1}^*) = 0$$

With the above derivation and Markov property, we have $I(\mathbf{o}_t; \mathbf{a}_t^* | \mathbf{s}_t, \mathbf{s}_{1:t-1}, \mathbf{a}_{1:t-1}) = 0$. We can generalize $\mathbf{a}_{1:t-1}^*$ to any $\mathbf{a}_{1:t-1}$ by assuming \mathbf{a}_t^* as the optimal action for state \mathbf{s}_t whose last timestep state-action pair is $(\mathbf{s}_{t-1}, \mathbf{a}_{t-1})$. Thus, we have \mathbf{s}_t is a sufficient representation for \mathbf{o}_t if and only if $\mathbf{s}_{1:T}$ is a sufficient representation of $\mathbf{o}_{1:T}$. \square

A.3. Multi-View Redundancy and Sufficiency

Proposition A.1. $\mathbf{o}_{1:T}^{(1)}$ is a redundant view with respect to $\mathbf{o}_{1:T}^{(2)}$ to obtain $\mathbf{a}_{1:T}^*$ if and only if $I(\mathbf{o}_{1:T}^{(1)}; \mathbf{a}_{1:T}^* | \mathbf{o}_{1:T}^{(2)}) = 0$. Any representation $\mathbf{s}_{1:T}^{(1)}$ of $\mathbf{o}_{1:T}^{(1)}$ that is sufficient for $\mathbf{o}_{1:T}^{(2)}$ is also sufficient for $\mathbf{a}_{1:T}^*$.

Proof. See proof of Proposition B.3 in the MIB paper (Federici et al., 2020). \square

Corollary A.1. Let $\mathbf{o}_{1:T}^{(1)}$ and $\mathbf{o}_{1:T}^{(2)}$ be two mutually redundant views for $\mathbf{a}_{1:T}^*$. Let $\mathbf{s}_{1:T}^{(1)}$ be a representation of $\mathbf{o}_{1:T}^{(1)}$. If $\mathbf{s}_{1:T}^{(1)}$ is sufficient for $\mathbf{o}_{1:T}^{(2)}$, $\mathbf{s}_t^{(1)}$ can derive \mathbf{a}_t^* as the joint observation of the two views ($I(\mathbf{o}_t^{(1)} \mathbf{o}_t^{(2)}; \mathbf{a}_t^* | \mathbf{s}_{t-1}, \mathbf{a}_{t-1}) = I(\mathbf{s}_t^{(1)}; \mathbf{a}_t^* | \mathbf{s}_{t-1}, \mathbf{a}_{t-1})$), where \mathbf{s}_{t-1} is any sufficient representation at timestep $t-1$.

Proof. For the sequential data, see proof of Corollary B.2.1 in the MIB paper (Federici et al., 2020) to prove

$$I(\mathbf{o}_{1:T}^{(1)} \mathbf{o}_{1:T}^{(2)}; \mathbf{a}_{1:T}^*) = I(\mathbf{s}_{1:T}^{(1)}; \mathbf{a}_{1:T}^*)$$

According to Theorem A.2, if $\mathbf{s}_{1:T}^{(1)}$ is a sufficient representation of $\mathbf{o}_{1:T}^{(2)}$, $\mathbf{s}_t^{(1)}$ is a sufficient representation of $\mathbf{o}_t^{(2)}$. Similar to proof on sequential data, we can use Corollary B.2.1 in the MIB paper (Federici et al., 2020) to show that

$$I(\mathbf{o}_t^{(1)} \mathbf{o}_t^{(2)}; \mathbf{a}_t^* | \mathbf{s}_{t-1}, \mathbf{a}_{t-1}) = I(\mathbf{s}_t^{(1)}; \mathbf{a}_t^* | \mathbf{s}_{t-1}, \mathbf{a}_{t-1})$$

\square

Theorem A.3. Let the two views $\mathbf{o}_{1:T}^{(1)}$ and $\mathbf{o}_{1:T}^{(2)}$ of observation $\mathbf{o}_{1:T}$ are obtained by data augmentation transformation sequences $t_{1:T}^{(1)}$ and $t_{1:T}^{(2)}$ respectively ($\mathbf{o}_{1:T}^{(1)} = t_{1:T}^{(1)}(\mathbf{o}_{1:T})$ and $\mathbf{o}_{1:T}^{(2)} = t_{1:T}^{(2)}(\mathbf{o}_{1:T})$). Whenever $I(t_{1:T}^{(1)}(\mathbf{o}_{1:T}); \mathbf{a}_{1:T}^*) = I(t_{1:T}^{(2)}(\mathbf{o}_{1:T}); \mathbf{a}_{1:T}^*) = I(\mathbf{o}_{1:T}; \mathbf{a}_{1:T}^*)$, the two views $\mathbf{o}_{1:T}^{(1)}$ and $\mathbf{o}_{1:T}^{(2)}$ must be mutually redundant for $\mathbf{a}_{1:T}^*$. Besides, the two views $\mathbf{o}_t^{(1)}$ and $\mathbf{o}_t^{(2)}$ must be mutually redundant for \mathbf{a}_t^* .

Proof. Let $\mathbf{s}_{1:T}$ be a sufficient representation for both original and multi-view observations. We first factorize the

mutual information and refer A.2 as Theorem A.2.

$$\begin{aligned} I(t_{1:t}^{(1)}(\mathbf{o}_{1:t}); \mathbf{a}_{1:t}^*) &= I(\mathbf{o}_{1:t}^{(1)}; \mathbf{a}_{1:t}^*) \\ \stackrel{\text{(P.2)}}{=} &I(\mathbf{o}_t^{(1)}; \mathbf{a}_{1:t}^* | \mathbf{o}_{1:t-1}^{(1)}) + I(\mathbf{o}_{1:t-1}^{(1)}; \mathbf{a}_{1:t}^*) \\ \stackrel{\text{A.2}}{=} &I(\mathbf{o}_t^{(1)}; \mathbf{a}_{1:t}^* | \mathbf{s}_{1:t-1}) + I(\mathbf{s}_{1:t-1}; \mathbf{a}_{1:t}^*) \end{aligned}$$

$$\begin{aligned} I(t_{1:t}^{(2)}(\mathbf{o}_{1:t}); \mathbf{a}_{1:t}^*) &= I(\mathbf{o}_{1:t}^{(2)}; \mathbf{a}_{1:t}^*) \\ \stackrel{\text{(P.2)}}{=} &I(\mathbf{o}_t^{(2)}; \mathbf{a}_{1:t}^* | \mathbf{o}_{1:t-1}^{(2)}) + I(\mathbf{o}_{1:t-1}^{(2)}; \mathbf{a}_{1:t}^*) \\ \stackrel{\text{A.2}}{=} &I(\mathbf{o}_t^{(2)}; \mathbf{a}_{1:t}^* | \mathbf{s}_{1:t-1}) + I(\mathbf{s}_{1:t-1}; \mathbf{a}_{1:t}^*) \end{aligned}$$

$$\begin{aligned} I(t_{1:t}^{(2)}(\mathbf{o}_{1:t}); \mathbf{a}_{1:t}^*) &= I(\mathbf{o}_{1:t}^{(2)}; \mathbf{a}_{1:t}^*) \\ \stackrel{\text{(P.2)}}{=} &I(\mathbf{o}_t^{(2)}; \mathbf{a}_{1:t}^* | \mathbf{o}_{1:t-1}^{(2)}) + I(\mathbf{o}_{1:t-1}^{(2)}; \mathbf{a}_{1:t}^*) \end{aligned}$$

$$\begin{aligned} I(\mathbf{o}_{1:t}; \mathbf{a}_{1:t}^*) &= I(\mathbf{o}_{1:t}; \mathbf{a}_{1:t}^*) \\ \stackrel{\text{(P.2)}}{=} &I(\mathbf{o}_t; \mathbf{a}_{1:t}^* | \mathbf{o}_{1:t-1}) + I(\mathbf{o}_{1:t-1}; \mathbf{a}_{1:t}^*) \\ \stackrel{\text{A.2}}{=} &I(\mathbf{o}_t; \mathbf{a}_{1:t}^* | \mathbf{s}_{1:t-1}) + I(\mathbf{s}_{1:t-1}; \mathbf{a}_{1:t}^*) \end{aligned}$$

Then, we have the following equality

$$I(\mathbf{o}_t^{(1)}; \mathbf{a}_{1:t}^* | \mathbf{s}_{1:t-1}) = I(\mathbf{o}_t^{(2)}; \mathbf{a}_{1:t}^* | \mathbf{s}_{1:t-1}) = I(\mathbf{o}_t; \mathbf{a}_{1:t}^* | \mathbf{s}_{1:t-1})$$

Similar as derivation in Theorem A.2

$$\begin{aligned} &I(\mathbf{o}_t^{(1)}; \mathbf{a}_{1:t}^* | \mathbf{s}_{1:t-1}) \\ \stackrel{\text{(P.2)}}{=} &I(\mathbf{o}_t^{(1)}; \mathbf{a}_t^* | \mathbf{a}_{1:t-1}^*, \mathbf{s}_{1:t-1}) + I(\mathbf{o}_t^{(1)}; \mathbf{a}_{1:t-1}^* | \mathbf{s}_{1:t-1}) \\ \stackrel{\text{Equation 10}}{=} &I(\mathbf{o}_t^{(1)}; \mathbf{a}_t^* | \mathbf{a}_{1:t-1}^*, \mathbf{s}_{1:t-1}) + I(\mathbf{s}_t; \mathbf{a}_{1:t-1}^* | \mathbf{s}_{1:t-1}) \end{aligned}$$

We apply the same derivation for $\mathbf{o}^{(2)}$ and \mathbf{o} , we have the following with Markov property

$$\begin{aligned} &I(t_t^{(1)}(\mathbf{o}_t); \mathbf{a}_t^* | \mathbf{s}_{t-1}, \mathbf{a}_{t-1}) \\ &= I(t_t^{(2)}(\mathbf{o}_t); \mathbf{a}_t^* | \mathbf{s}_{t-1}, \mathbf{a}_{t-1}) \\ &= I(\mathbf{o}_t; \mathbf{a}_t^* | \mathbf{s}_{t-1}, \mathbf{a}_{t-1}) \end{aligned}$$

We show that the condition on sequential data can be expressed at each timestep with the similar form. See proof of Proposition B.4 in the MIB paper (Federici et al., 2020) for mutual redundancy between sequential views and individual pairs of views. \square

Theorem A.4. Suppose the mutually redundant condition holds, i.e. $I(t_{1:T}^{(1)}(\mathbf{o}_{1:T}); \mathbf{a}_{1:T}^*) = I(t_{1:T}^{(2)}(\mathbf{o}_{1:T}); \mathbf{a}_{1:T}^*) = I(\mathbf{o}_{1:T}; \mathbf{a}_{1:T}^*)$. If $\mathbf{s}_{1:T}^{(1)}$ is a sufficient representation for $t_{1:T}^{(1)}(\mathbf{o}_{1:T})$ then $I(\mathbf{o}_t; \mathbf{a}_t^* | \mathbf{s}_{t-1}, \mathbf{a}_{t-1}) = I(\mathbf{s}_t^{(1)}; \mathbf{a}_t^* | \mathbf{s}_{t-1}, \mathbf{a}_{t-1})$.

Proof. Since $t_{1:T}^{(1)}(\mathbf{o}_{1:T})$ is redundant for $t_{1:T}^{(2)}(\mathbf{o}_{1:T})$ (Theorem A.3), any representation $\mathbf{s}_t^{(1)}$ of $t_{1:T}^{(1)}(\mathbf{o}_{1:T})$ that is sufficient for $t_{1:T}^{(2)}(\mathbf{o}_{1:T})$ must also be sufficient for \mathbf{a}_t^* (Theorem A.2 and Proposition A.1). Using Theorem A.2 we have $I(\mathbf{s}_t^{(1)}; \mathbf{a}_t^* | \mathbf{s}_{t-1}, \mathbf{a}_{t-1}) = I(t_t^{(1)}(\mathbf{o}_t); \mathbf{a}_t^* | \mathbf{s}_{t-1}, \mathbf{a}_{t-1})$. With $I(t_t^{(1)}(\mathbf{o}_t); \mathbf{a}_t^* | \mathbf{s}_{t-1}, \mathbf{a}_{t-1}) = I(\mathbf{o}_t; \mathbf{a}_t^* | \mathbf{s}_{t-1}, \mathbf{a}_{t-1})$, we conclude $I(\mathbf{o}_t; \mathbf{a}_t^* | \mathbf{s}_{t-1}, \mathbf{a}_{t-1}) = I(\mathbf{s}_t^{(1)}; \mathbf{a}_t^* | \mathbf{s}_{t-1}, \mathbf{a}_{t-1})$. \square

We finally show the proposition for the Multi-Information Bottleneck principle in RL with the generalization of sufficiency and mutually redundancy condition from sequential data to each individual pairs of data.

Proposition A.2. Let $\mathbf{o}_t^{(1)}$ and $\mathbf{o}_t^{(2)}$ be mutually redundant views for \mathbf{a}_t^* that share only optimal action information. Then a sufficient representation of $\mathbf{s}_t^{(1)}$ of $\mathbf{o}_t^{(1)}$ for $\mathbf{o}_t^{(2)}$ that is minimal for $\mathbf{o}_t^{(2)}$ is also a minimal representation for \mathbf{a}_t^* .

Proof. See proof of Proposition E.1 in the MIB paper (Federici et al., 2020). \square

B. DRIBO Loss Computation

We consider the average of the information bottleneck losses from the two views.

$$\begin{aligned} &\mathcal{L}_{\frac{1+2}{2}} \tag{11} \\ &= \frac{I(\mathbf{s}_t^{(1)}; \mathbf{o}_t^{(1)} | \mathbf{s}_{t-1}^{(1)}, \mathbf{a}_{t-1}, \mathbf{o}_t^{(2)}) + I(\mathbf{s}_t^{(2)}; \mathbf{o}_t^{(2)} | \mathbf{s}_{t-1}^{(2)}, \mathbf{a}_{t-1}, \mathbf{o}_t^{(1)})}{2} \\ &\quad - \frac{\lambda_1 I(\mathbf{s}_t^{(1)}; \mathbf{o}_t^{(2)} | \mathbf{s}_{t-1}^{(1)}, \mathbf{a}_{t-1}) + \lambda_2 I(\mathbf{s}_t^{(2)}; \mathbf{o}_t^{(1)} | \mathbf{s}_{t-1}^{(2)}, \mathbf{a}_{t-1})}{2} \tag{12} \end{aligned}$$

Consider $\mathbf{s}_t^{(1)}$ and $\mathbf{s}_t^{(2)}$ on the same domain \mathbb{S} , $I(\mathbf{s}_t^{(1)}; \mathbf{o}_t^{(1)} | \mathbf{s}_{t-1}^{(1)}, \mathbf{a}_{t-1}, \mathbf{o}_t^{(2)})$ can be expressed as:

$$\begin{aligned} &I(\mathbf{s}_t^{(1)}; \mathbf{o}_t^{(1)} | \mathbf{s}_{t-1}^{(1)}, \mathbf{a}_{t-1}, \mathbf{o}_t^{(2)}) \\ &= \mathbb{E} \left[\log \frac{p_\theta(\mathbf{s}_t^{(1)} | \mathbf{o}_t^{(1)}, \mathbf{s}_{t-1}^{(1)}, \mathbf{a}_{t-1})}{p_\theta(\mathbf{s}_t^{(1)} | \mathbf{o}_t^{(2)}, \mathbf{s}_{t-1}^{(1)}, \mathbf{a}_{t-1})} \right] \\ &= \mathbb{E} \left[\log \frac{p_\theta(\mathbf{s}_t^{(1)} | \mathbf{o}_t^{(1)}, \mathbf{s}_{t-1}^{(1)}, \mathbf{a}_{t-1}) p_\theta(\mathbf{s}_t^{(2)} | \mathbf{o}_t^{(2)}, \mathbf{s}_{t-1}^{(2)}, \mathbf{a}_{t-1})}{p_\theta(\mathbf{s}_t^{(2)} | \mathbf{o}_t^{(2)}, \mathbf{s}_{t-1}^{(2)}, \mathbf{a}_{t-1}) p_\theta(\mathbf{s}_t^{(1)} | \mathbf{o}_t^{(2)}, \mathbf{s}_{t-1}^{(1)}, \mathbf{a}_{t-1})} \right] \\ &= D_{\text{KL}}(p_\theta(\mathbf{s}_t^{(1)} | \mathbf{o}_t^{(1)}, \mathbf{s}_{t-1}^{(1)}, \mathbf{a}_{t-1}) || p_\theta(\mathbf{s}_t^{(2)} | \mathbf{o}_t^{(2)}, \mathbf{s}_{t-1}^{(2)}, \mathbf{a}_{t-1})) \\ &\quad - D_{\text{KL}}(p_\theta(\mathbf{s}_t^{(1)} | \mathbf{o}_t^{(2)}, \mathbf{s}_{t-1}^{(1)}, \mathbf{a}_{t-1}) || p_\theta(\mathbf{s}_t^{(2)} | \mathbf{o}_t^{(2)}, \mathbf{s}_{t-1}^{(2)}, \mathbf{a}_{t-1})) \\ &\leq D_{\text{KL}}(p_\theta(\mathbf{s}_t^{(1)} | \mathbf{o}_t^{(1)}, \mathbf{s}_{t-1}^{(1)}, \mathbf{a}_{t-1}) || p_\theta(\mathbf{s}_t^{(2)} | \mathbf{o}_t^{(2)}, \mathbf{s}_{t-1}^{(2)}, \mathbf{a}_{t-1})) \tag{13} \end{aligned}$$

Note that equality holds if the two distributions coincide. Analogously

$I(\mathbf{s}_t^{(2)}; \mathbf{o}_t^{(2)} | \mathbf{s}_{t-1}^{(2)}, \mathbf{a}_{t-1}, \mathbf{o}_t^{(1)})$ is upper bounded by $D_{\text{KL}}(p_{\theta}(\mathbf{s}_t^{(2)} | \mathbf{o}_t^{(2)}, \mathbf{s}_{t-1}^{(2)}, \mathbf{a}_{t-1}) || p_{\theta}(\mathbf{s}_t^{(1)} | \mathbf{o}_t^{(1)}, \mathbf{s}_{t-1}^{(1)}, \mathbf{a}_{t-1}))$.

Assume \mathbf{s}_{t-1} is a sufficient representation of \mathbf{o}_{t-1} . Then, $\mathbf{s}_{t-1}^{(1)}$ provides task-relevant information no more than the sufficient representation \mathbf{s}_{t-1} . $I(\mathbf{s}_t^{(1)}; \mathbf{o}_t^{(2)} | \mathbf{s}_{t-1}^{(1)}, \mathbf{a}_{t-1})$ can be thus re-expressed as:

$$\begin{aligned}
 & I(\mathbf{s}_t^{(1)}; \mathbf{o}_t^{(2)} | \mathbf{s}_{t-1}^{(1)}, \mathbf{a}_{t-1}) \\
 & \geq I(\mathbf{s}_t^{(1)}; \mathbf{o}_t^{(2)} | \mathbf{s}_{t-1}, \mathbf{a}_{t-1}) \\
 & \stackrel{(P.2)}{=} I(\mathbf{s}_t^{(1)}; \mathbf{s}_t^{(2)} \mathbf{o}_t^{(2)} | \mathbf{s}_{t-1}, \mathbf{a}_{t-1}) - I(\mathbf{s}_t^{(1)}; \mathbf{s}_t^{(2)} | \mathbf{o}_t^{(2)}, \mathbf{s}_{t-1}, \mathbf{a}_{t-1}) \\
 & \stackrel{*}{=} I(\mathbf{s}_t^{(1)}; \mathbf{s}_t^{(2)} \mathbf{o}_t^{(2)} | \mathbf{s}_{t-1}, \mathbf{a}_{t-1}) \\
 & = I(\mathbf{s}_t^{(1)}; \mathbf{s}_t^{(2)} | \mathbf{s}_{t-1}, \mathbf{a}_{t-1}) + I(\mathbf{s}_t^{(1)}; \mathbf{o}_t^{(2)} | \mathbf{s}_t^{(2)}, \mathbf{s}_{t-1}, \mathbf{a}_{t-1}) \\
 & \geq I(\mathbf{s}_t^{(1)}; \mathbf{s}_t^{(2)} | \mathbf{s}_{t-1}, \mathbf{a}_{t-1}) \tag{14}
 \end{aligned}$$

Where $*$ follows from $\mathbf{s}_t^{(2)}$ being the representation of $\mathbf{o}_t^{(2)}$. The bound is tight whenever $\mathbf{s}_t^{(2)}$ is sufficient from $\mathbf{s}_t^{(1)}$ ($I(\mathbf{s}_t^{(1)}; \mathbf{o}_t^{(1)} | \mathbf{s}_{t-1}, \mathbf{a}_{t-1}, \mathbf{o}_t^{(2)}) = 0$). This happens whenever $\mathbf{s}_t^{(2)}$ contains all the information regarding $\mathbf{s}_t^{(1)}$. Once again, we can have $I(\mathbf{s}_t^{(2)}; \mathbf{o}_t^{(1)} | \mathbf{s}_{t-1}^{(2)}, \mathbf{a}_{t-1}) \geq I(\mathbf{s}_t^{(1)}; \mathbf{s}_t^{(2)} | \mathbf{s}_{t-1}, \mathbf{a}_{t-1})$. Therefore, the averaged loss functions can be upper-bounded by

$$\begin{aligned}
 \mathcal{L}_{\frac{1+2}{2}} & \leq -\frac{\lambda_1 + \lambda_2}{2} I(\mathbf{s}_t^{(1)}; \mathbf{s}_t^{(2)} | \mathbf{s}_{t-1}, \mathbf{a}_{t-1}) \\
 & + D_{\text{SKL}}(p_{\theta}(\mathbf{s}_t^{(1)} | \mathbf{o}_t^{(1)}, \mathbf{s}_{t-1}^{(1)}, \mathbf{a}_{t-1}) || p_{\theta}(\mathbf{s}_t^{(2)} | \mathbf{o}_t^{(2)}, \mathbf{s}_{t-1}^{(2)}, \mathbf{a}_{t-1})) \tag{15}
 \end{aligned}$$

Lastly, by re-parametrizing the objective, we obtain:

$$\begin{aligned}
 \mathcal{L}(\theta; \beta) & = -I_{\theta}(\mathbf{s}_t^{(1)}; \mathbf{s}_t^{(2)} | \mathbf{s}_{t-1}, \mathbf{a}_{t-1}) \\
 & + \beta D_{\text{SKL}}(p_{\theta}(\mathbf{s}_t^{(1)} | \mathbf{o}_t^{(1)}, \mathbf{s}_{t-1}^{(1)}, \mathbf{a}_{t-1}) || p_{\theta}(\mathbf{s}_t^{(2)} | \mathbf{o}_t^{(2)}, \mathbf{s}_{t-1}^{(2)}, \mathbf{a}_{t-1})) \tag{16}
 \end{aligned}$$

In Algorithm 1, we use $\mathbf{s}_t^{(1)} \sim p_{\theta}(\mathbf{s}_t^{(1)} | \mathbf{o}_t^{(1)}, \mathbf{s}_{t-1}^{(1)}, \mathbf{a}_{t-1})$ and $\mathbf{s}_t^{(2)} \sim p_{\theta}(\mathbf{s}_t^{(2)} | \mathbf{o}_t^{(2)}, \mathbf{s}_{t-1}^{(2)}, \mathbf{a}_{t-1})$ to obtain representations for multi-view observations. We argue that the substitution does not affect the effectiveness of the averaged objective. With the multi-view assumption, we have that representations $\mathbf{s}_{t-1}^{(1)}$ and $\mathbf{s}_{t-1}^{(2)}$ do not share any task-irrelevant information. So, the representations at timestep t conditioned on them do not share any task-irrelevant information. Maximizing the mutual information between $\mathbf{s}_t^{(1)}$ and $\mathbf{s}_t^{(2)}$ (first term in Equation 16) will encourage the representations to share maximal task-relevant information. Similar

argument also works for the second term in Equation 16. Since $\mathbf{s}_{t-1}^{(1)}$ and $\mathbf{s}_{t-1}^{(2)}$ do not share any task-irrelevant information, any task-irrelevant information introduced from the conditional probability will be also identified as task-irrelevant information by KL divergence, which will be reduced through minimizing the DRIBO loss.

C. Implementation Details

C.1. DRIBO + SAC

We first show how we train SAC agent given the representations of DRIBO. Let $\phi(\mathbf{o}) = \mathbf{s} \sim p_{\theta}(\mathbf{s} | \mathbf{o}, \mathbf{s}', \mathbf{a}')$ denote the encoder, where \mathbf{s}' and \mathbf{a}' as the representation and action at last timestep.

Algorithm 2 SAC + DRIBO Encoder

input RL batch $\mathcal{B}_{\text{RL}} = \{(\phi(\mathbf{o}_i), a_i, r_i, \phi(\mathbf{o}'_i))\}_{i=1}^{(T-1)*N}$ with $(T-1)*N$ pairs of representation, action, reward and next representation.

- 1: Get value: $V = \min_{i=1,2} \hat{Q}_i(\hat{\phi}(\mathbf{o}')) - \alpha \log \pi(a | \hat{\phi}(\mathbf{o}'))$
- 2: Train critics: $J(Q_i, \phi) = (Q_i(\phi(\mathbf{o})) - r - \gamma V)^2$
- 3: Train actor: $J(\pi) = \alpha \log \pi(a | \phi(\mathbf{o})) - \min_{i=1,2} Q_i(\phi(\mathbf{o}))$
- 4: Train alpha: $J(\alpha) = -\alpha \log \pi(a | \phi(\mathbf{o})) - \alpha \mathcal{H}(a | \phi(\mathbf{o}))$
- 5: Update target critics: $\hat{Q}_i = \tau_Q Q_i + (1 - \tau_Q) \hat{Q}_i$
- 6: Update target encoder: $\hat{\phi} \leftarrow \tau_{\phi} \phi + (1 - \tau_{\phi}) \phi$

Then we incorporate the above SAC algorithm into minimizing DRIBO loss as follows:

Algorithm 3 DRIBO + SAC

input : Replay buffer \mathcal{D} storing sequential observations and actions with length T . The batch size is N . The number of total training step is K . The number of total episodes is E .

- 1: **for** $e = 1, \dots, E$ **do**
- 2: Sample sequential observations and actions from the environment and append new samples to \mathcal{D} .
- 3: **for** each step $k = 1, \dots, K$ **do**
- 4: Sample a sequential batch $\mathcal{B} \sim \mathcal{D}$.
- 5: Compute the representations batch \mathcal{B}_{RL} which has the shape (T, N) using the encoder $p_{\theta}(\mathbf{s}_{1:T} | \mathbf{o}_{1:T}, \mathbf{a}_{1:T})$
- 6: Train SAC agent: $\mathbb{E}_{\mathcal{B}_{\text{RL}}} [J(\pi, Q, \phi)]$ {Algorithm 2}
- 7: Update θ and ψ to minimize $\mathcal{L}_{\text{DRIBO}}$ using \mathcal{B} {Algorithm 1}.
- 8: **end for**
- 9: **end for**

C.2. DRIBO + PPO

The main difference between SAC and PPO is that PPO is an on-policy RL algorithm while SAC is an off-policy RL algorithm. With the update of the encoder, representations may not be consistent within each training step which breaks the on-policy sampling assumption. To address this issue, instead of obtaining s_t propagating from the initial observation of the observation sequence, we store the representations as s_t^{old} while sampling from the on-policy batch. Then, we use $\varphi(o) = s \sim p_\theta(s|o, s^{\text{old}}, a')$ to denote the representation from the encoder. Here, s^{old} and a' are the representation and action at the previous timestep. By treating the encoding process as a part of the policy and value function, the on-policy requirement is satisfied since the new action/value at timestep t depends only on $(o_t, s_{t-1}^{\text{old}}, a_{t-1})$.

Algorithm 4 DRIBO + PPO

```

input : Replay buffer  $\mathcal{D}$  and on-policy replay buffer  $\mathcal{D}_{\text{PPO}}$ 
    storing sequential observations and actions with length
     $T$ . The batch size is  $N$ . The minibatch size for PPO is
     $M$ . The number of total episodes is  $E$ .
1: for  $e = 1, \dots, E$  do
2:   Sample sequential observations and actions from the
      environment  $\{(o_{1:T}, a_{1:T}, r_{1:T}, s_{1:T}^{\text{old}}\}_{i=1}^N$ .
3:   Append new samples to  $\mathcal{D}$  and update the on-policy
      replay buffer  $\mathcal{D}_{\text{PPO}}$ .
4:   for  $j = 1, \dots, M$  do
5:      $\{(\varphi(o_i), a_i, r_i)\}_{i=1}^{\lfloor \frac{T*N}{M} \rfloor} \sim \mathcal{D}_{\text{PPO}}$ 
6:     Optimize PPO policy, value function and encoder
      using each sample  $(\varphi(o_i), a_i, r_i)$  in the batch.
7:   Sample a sequential batch  $\mathcal{B} \sim \mathcal{D}$ .
8:   Update  $\theta$  and  $\psi$  to minimize  $\mathcal{L}_{\text{DRIBO}}$  using  $\mathcal{B}$ 
      {Algorithm 1}.
9: end for
10: end for

```

C.3. DMC

We use the same encoder architecture as the encoder in the RSSM paper (Hafner et al., 2019). Deterministic part of the representation is a 200-dimensional vector. Stochastic part of the representation is a 30-dimensional diagonal Gaussian with predicted mean and standard deviation. Thus, the representation is a 230-dimensional vector. We implement Q-network and policy in SAC as MLPs with two fully connected layers of size 1024 with ReLU activations. The mutual information (MI) estimator $I_\psi(s^{(1)}, s^{(2)})$ is a MLP with two fully connected layers of size 500 with ReLU activations.

Augmentations of Visual Observations. For our approach DRIBO and RAD, we use *crop+random grayscale* to gener-

ate multi-view observations and augmented data. We apply the implementation of RAD to do the augmentation. For *crop*, it extracts a random patch from the original observation. In DMC, we render 100×100 pixel observations and crop randomly to 84×84 pixels. We then resize the cropped observations to 100×100 pixels. For *random grayscale*, it converts RGB images to grayscale with a probability $p=0.3$.

Hyperparameters. To facilitate the optimization, the hyperparameter β in the DRIBO loss Algorithm 1 is slowly increased during training. β value starts from a small value $1e-8$ and increases to $1e-3$ with an exponential scheduler. The same procedure is also used in the MIB paper (Federici et al., 2020). We show other hyperparameters for DMC experiments in Table 2.

Table 2: Hyperparameters used for DMC experiments.

Hyperparameters	Value
Observation size	(100×100)
Replay buffer size	1000000
Initial steps	1000
Stacked frames	No
Action repeat	2 finger, spin; walker, stand, walk, run; 4 otherwise
Evaluation episodes	8
Optimizer	Adam
Learning rate	encoder learning rate: $1e-4$; MI estimator learning rate: $1e-4$; policy/Q network learning rate: $1e-3$; α learning rate: $1e-4$.
Batch size	10×50 , where $T = 50$
Target update τ	0.005
Target update freq	2
Discount γ	.99
Initial temperature	0.1
Num. of steps per episode	1000
Num. of training steps per episode	500
β scheduler start episode	10
β scheduler end episode	110

C.4. Progen

For Progen suite, the implementation of DRIBO is almost the same as DMC experiments. Better design choice could be found by validation. We use the same as the encoder architecture used in DMC experiments, except for the observation embedder, which we use the network from IMPALA paper to take the visual observations. In addition, since the actions in Progen suite are discrete, we use an action embedder to embed discrete actions into continuous space. The action embedder is implemented as a simple one hidden layer resblock with 64 neurons. It maps a one-hot action vector to a 4-dimensional vector. The policy and value function share one hidden layer with 1024 neurons. The policy uses another fully connected layer to generate a categorical distribution to select the discrete action. The value function uses another fully connected layer to generate the value for an input representation. All activation functions are ReLU

activations.

Augmentation of Visual Observations. We select augmentation types based on the best reported augmentation types for each environment. DrAC (Raileanu et al., 2020) reported best augmentation types for RAD and DrAC in Table 4 and 5 of the DrAC paper. We list the augmentation types used in DRIBO in Table 3 and 4. We use the same settings for each augmentation type as DrAC. Note that we only performed limited experiments to select the augmentations reported in the tables due to time constraints. So, the tables do not show the best augmentation types in each environment for DRIBO.

Table 3: Augmentation type used for each game.

Env	BigFish	StarPilot	FruitBot	BossFight	Ninja	Plunder	CaveFlyer	CoinRun
Augmentation	crop	cutout	cutout	cutout	random-conv	crop	random-conv	random-conv

Table 4: Augmentation type used for each game.

Env	Jumper	Chaser	Climber	DodgeBall	Heist	Leaper	Maze	Miner
Augmentation	random-conv	crop	random-conv	cutout	crop	crop	crop	flip

Hyperparameters. We use the same β scheduler as the DMC experiments. The starting β value is $1e - 8$ and the final β value is $1e - 3$ (the same as DMC experiments). We show other hyperparameters for Procgen environments in Table 5.

Table 5: Hyperparameters used for Procgen experiments.

Hyperparameters	Value
Observation size	(64×64)
Replay buffer size	1000000
Num. of steps per rollout	256
Num. of epochs per rollout	3
Num. of minibatches per epoch	8
Stacked frames	No
Evaluation episodes	10
Optimizer	Adam
Learning rate	encoder learning rate: $1e-4$; MI estimator learning rate: $1e-4$; policy learning rate: $5e-4$; α learning rate: $1e-4$.
Batch size	8×256 , where $T = 256$
Entropy bonus	0.01
PPO clip range	0.2
Discount γ	.99
GAE parameter λ	0.95
Reward normalization	yes
Num. of workers	1
Num. of environments per worker	64
Total timesteps	25M
β scheduler start episode	10
β scheduler end episode	110

Discussion. Here, we extend the discussion on why our method underperforms on some environments, whose screenshots are shown in Figure 6.

Our approach, DRIBO, only consider global MI (Hjelm et al., 2019) in the current implementation. As a result, local structures can be easily ignored in the representation. More specifically, representations containing the same static local features within a single execution but at different timesteps are treated as negative examples in the mutual information maximization. Then, the information of these local features shared between representations is not maximized. Negative pairs of representations sharing this type of local features are globally negative pairs but locally positive pairs.

For Plunder, the goal is to destroy moving enemy pirate ships by firing cannonballs. The enemy ships can be identified with the color of the target in the bottom left corner. The background of the game maintains the same within a single execution. Wooden obstacles capable of blocking the player’s cannonballs. In a single execution, critical features like the target label and wooden obstacles remain unchanged. Failing to capture these local features results in poor performance of an agent.

For Chaser, the goal is to collect all green orbs as well as stars. A collision with an enemy that is not vulnerable (red) results in the death of the player. The background remains the same across different executions. Walls in the environment are dense and remain static during a single execution. Failing to capture walls’ positions in representations hinders the agent from navigating to avoid enemies and collect orbs/stars. In Maze and Leaper, walls also remain static, but the backgrounds are different across different executions. This difference reduces the influence introduced by globally negative pairs but locally positive pairs. By contrast, walls in DodgeBall remain static but more critical since hitting at a wall ends the game.

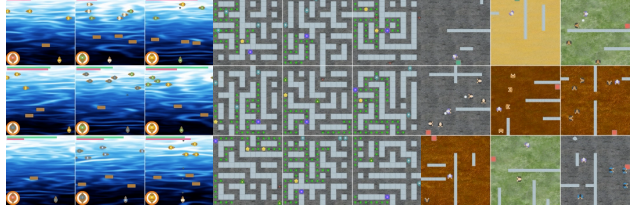


Figure 6: Screenshots of the three Procgen games where our approach DRIBO does not improve generalization performance compared to the other methods. From left to right, they are Plunder, Chaser and DodgeBall.